Noncollinear Magnetic Structure and Multipolar Order in $Eu_2Ir_2O_7$

Yilin Wang,[1] Hongming Weng,[1] Liang Fu,[2] and Xi Dai[1,3,4]
[1]*Beijing National Laboratory for Condensed Matter Physics, and Institute of Physics, Chinese Academy of Sciences, Beijing 100190, China*
[2]*Department of Physics, Massachusetts Institute of Technology, Cambridge, Massachusetts 02139, USA*
[3]*Collaborative Innovation Center of Quantum Matter, Beijing 100190, China*
[4]*Department of Physics, Hong Kong University of Science and Technology, Clear Water Bay, Hong Kong, China*
(Received 15 May 2017; published 2 November 2017)

The magnetic properties of the pyrochlore iridate material $Eu_2Ir_2O_7$ ($5d^5$) have been studied based on first principles calculations, where the crystal field splitting Δ, spin-orbit coupling (SOC) λ, and Coulomb interaction U within Ir $5d$ orbitals all play significant roles. The ground state phase diagram has been obtained with respect to the strength of SOC and Coulomb interaction U, where a stable antiferromagnetic ground state with all-in–all-out (AIAO) spin structure has been found. In addition, another antiferromagnetic state with energy close to AIAO has also been found to be stable. The calculated nonlinear magnetization of the two stable states both have the d-wave pattern but with a $\pi/4$ phase difference, which can perfectly explain the experimentally observed nonlinear magnetization pattern. Compared with the results of the nondistorted structure, it turns out that the trigonal lattice distortion is crucial for stabilizing the AIAO state in $Eu_2Ir_2O_7$. Furthermore, besides large dipolar moments, we also find considerable octupolar moments in the magnetic states.

DOI: 10.1103/PhysRevLett.119.187203

The ordering of electronic states is one of the fundamental problems in condensed matter physics. In $3d$ transition metal compounds, the ordered states can be described quite well by the product of orders in orbital and spin subspaces [1], because the spin-orbit coupling (SOC) here is weak and can be treated perturbatively. However, in rare-earth compounds [2], the SOC is strong enough to bind the orbital and spin degrees of freedom into rigid objects described by the total angular momentum, and the ordered states can then be well understood in terms of the moments with high angular momentum that splits into atomic multiplets under crystal field. Unlike the above two limits, the situation in $4d$ and $5d$ transition metal compounds is unique [3]. On one hand, the SOC is strong enough to combine the orbital and spin degrees of freedom to form some complex orders. While on the other hand, the SOC is still far away from the limit where the low energy physics can be entirely determined within the subspace with a fixed total angular momentum. In fact, the SOC strength in these compounds is comparable to that of the crystal field so that the magnetic orders there can involve multiple total angular momentum states.

The pyrochlore iridates [4,5] are typical $5d$ transition metal compounds with many novel properties already being discussed extensively in the literature, including the noncollinear magnetic order [6–12], the metal-insulator transition [13–20], the anomalous Hall effect [21–23], the topological insulator and the Weyl semimetal phase [3,6,7,15,24–31], and the chiral metallic states in the domain wall [32–34]. Among them, the magnetic order is the most fundamental one that determines most of the electronic properties. In Ref. [6], by using the density functional theory plus U (DFT + U) method, Wan *et al.* obtained an all-in–all-out (AIAO) order in $Y_2Ir_2O_7$, which will generate the Weyl semimetal phase if the value of the order parameter falls into a proper region. Most recently, Liang *et al.* [35] have systematically studied the nonlinear magnetization in $Eu_2Ir_2O_7$ ($5d^5$) by using torque magnetometry, where a magnetic field is applied in the a-b plane and continuously rotated around the c axis by 2π. They found a nonlinear magnetization normal to the a-b plane with a d-wave pattern as a function of the rotation angle. Surprisingly, they also found that the d-wave pattern has a $\pi/4$ phase shift when the direction of the field $\boldsymbol{H}_{\mathrm{fc}}$ applied during the field cooling process changes from $[\bar{1}\,\bar{1}\,0]$ to $[\bar{1}10]$. Their results indicate that there is another low energy metastable magnetic structure besides AIAO which might be stabilized by the field cooling processes.

Inspired by experiments on the nonlinear magnetization in $Eu_2Ir_2O_7$ [35], in the present Letter we reexamine the magnetic structure of the pyrochlore iridates. By using the DFT together with the unrestricted Hartree-Fock (UHF) mean-field method, we study the full description of the magnetic orders in $Eu_2Ir_2O_7$. Our numerical studies lead to three important conclusions listed below. (i) Besides AIAO there is an additional locally stable magnetic structure in this system, which is very close to AIAO in energy. The existence of this additional metastable magnetic state can perfectly explain the puzzle in the nonlinear magnetization measurements [35]. (ii) The real ground state of $Eu_2Ir_2O_7$ is extremely sensitive to the trigonal lattice distortion of the pyrochlore structure and AIAO magnetic state can be

stabilized only with large enough trigonal distortion. (iii) In all these magnetic states mentioned above, in addition to the magnetic dipolar moments, we also find high-order multipolar moments (octupole) [2] with considerable amplitude as well. Recently, possible nondipolar hidden order has also been implied from the second harmonic generation (SHG) experiments on Sr_2IrO_4 [36]. The major difference between the multipolar orders discussed in Sr_2IrO_4 [36] and that in the present Letter is that the former one breaks the inversion symmetry. Because of the similarity in the local electronic structure, the results obtained in the present study may also be helpful in revealing the microscopic origin of the hidden orders in Sr_2IrO_4.

We take the experimental lattice parameters of $Eu_2Ir_2O_7$ from Ref. [37], that is $a = 10.243$ Å and $x = 0.3334$. For this x value, the oxygen octahedron has a trigonal distortion (compression along the local [111] direction). We also do calculations for the nondistorted structure ($x = 5/16$) for comparison. The DFT part of the calculations have been done by the Vienna *ab initio* simulation package (VASP) [38]. A tight binding (TB) Hamiltonian consisting of t_{2g} orbitals from four Ir atoms is then obtained from the non-SOC DFT calculation by the maximally localized Wannier functions method [39,40]. The t_{2g} orbitals are defined with respect to the local oxygen octahedron XYZ coordinate [41]. An atomic SOC term is added to the TB Hamiltonian to account for the strong SOC of Ir atoms with its strength λ being determined by fitting the first principles results. To consider the strong Coulomb interaction among Ir t_{2g} orbitals, an on-site Coulomb interaction term U is included. The total Hamiltonian can be written as

$$H = \sum_{\substack{jR'\beta \\ iR\alpha}} t_{ij}^{R\alpha,R'\beta} d_{iR\alpha}^{\dagger} d_{jR'\beta} + \lambda \sum_{iR\alpha\beta} (\vec{\mathbf{l}}_R \cdot \vec{\mathbf{s}}_R)_{\alpha\beta} d_{R\alpha}^{\dagger} d_{R\beta} + \frac{U}{2} \sum_{iR\alpha\beta\delta\gamma} d_{R\alpha}^{\dagger} d_{R\beta}^{\dagger} d_{R\delta} d_{R\gamma}, \quad (1)$$

where, i, j are the indices of primitive cell, R, $R' = 1, 2, 3, 4$ are the indices of Ir sites, and α, β, δ, γ are the combined orbital-spin indices. Under the UHF approximation, the Coulomb interaction terms are approximated as

$$d_{R\alpha}^{\dagger} d_{R\beta}^{\dagger} d_{R\delta} d_{R\gamma} \approx \rho_{\beta\delta}^{R} d_{R\alpha}^{\dagger} d_{R\gamma} + \rho_{\alpha\gamma}^{R} d_{R\beta}^{\dagger} d_{R\delta} - \rho_{\beta\gamma}^{R} d_{R\alpha}^{\dagger} d_{R\delta} - \rho_{\alpha\delta}^{R} d_{R\beta}^{\dagger} d_{R\gamma} - \rho_{\beta\delta}^{R} \rho_{\alpha\gamma}^{R} + \rho_{\beta\gamma}^{R} \rho_{\alpha\delta}^{R}, \quad (2)$$

where, $\rho_{\alpha\beta}^{R} = \langle d_{R\alpha}^{\dagger} d_{R\beta} \rangle$ is the local density matrix for the Ir atom at site R and is determined self-consistently. This TB + UHF method is numerically more stable than the *ab initio* DFT + U method and the total energy can converge to very high accuracy (~0.01 meV) [41].

The local density matrix obtained above gives the complete description of the magnetic orders in $Eu_2Ir_2O_7$. It can be decomposed into 36 single-particle irreducible tensor (or multipolar) operators $O_{K_1K_2}^{KM}$ defined in the spin-orbital space [2,49],

$$\rho^R = \sum_{K_1K_2KM} C_{K_1K_2}^{KM} O_{K_1K_2}^{KM}, \quad (3)$$

$$C_{K_1K_2}^{KM} = \mathrm{Tr}[\rho^R (O_{K_1K_2}^{KM})^{\dagger}]. \quad (4)$$

Note that all of these operators are defined with respect to the local [111] xyz coordinate [41] for each Ir atom; i.e., z is along the local [111] direction. These 36 operators serve as the complete set of the possible order parameters (OPs) and the details of their definition can be found in the Supplemental Material [41].

The phase diagrams with respect to the strength of SOC λ and Coulomb interaction U for both the distorted and nondistorted structures are obtained and shown in Fig. 2. With SOC, the t_{2g} bands will be split into $j_{\mathrm{eff}} = 1/2$ and $j_{\mathrm{eff}} = 3/2$ subbands, and the $j_{\mathrm{eff}} = 1/2$ subbands are half-filled. For small U, the ground state is paramagnetic, which is unstable against magnetic order when U reaches to some critical value. Assume that the magnetic unit cell does not enlarge, all the possible magnetic structures in $Eu_2Ir_2O_7$ can be classified by finding the magnetic co-representation for the tetrahedron group, which leads to $c\Gamma_{\mathrm{mag}} = 1c\Gamma_{3+} + 1c\Gamma_{5+} + 1c\Gamma_{7+} + 2c\Gamma_{9+}$ [50]. We have tried all these possible magnetic configurations in our calculations to determine the most stable magnetic order.

Figure 2(a) is the phase diagram for the experimental structure of $Eu_2Ir_2O_7$, which contains finite trigonal distortion. The typical band structures of each phase have been plotted in the Supplemental Material [41]. We find that the one-dimensional $c\Gamma_{3+}$ representation with an AIAO type antiferromagnetic configuration [AF1 in Fig. 1(a)] is always the ground magnetic state, which is quite consistent with the previous studies [51–53]. Similar to the results obtained in Refs. [6,7], under the AF1 order, a Weyl semimetal phase can be found in a narrow region of the phase diagram. With the increment of U, the Weyl semimetal phase disappears quickly leading to a semimetal to insulator transition. Besides $c\Gamma_{3+}$, we find that the three-dimensional $c\Gamma_{7+}$ representation [AF3 in Figs. 1(d), 1(e), 1(f)], where the local moments are perpendicular to the local [111] directions, is also stable in the very large parameter region. However, its total energy per Ir atom is always a few meV higher than that of AF1 and a color map is used to label their total energy difference: $E_{\mathrm{tot}}(\mathrm{AF3}) - E_{\mathrm{tot}}(\mathrm{AF1})$ (with units of meV) in Fig. 2. As we can see, their total energy is very close. We choose the reasonable parameters for $Eu_2Ir_2O_7$ based on the size of the band gap reported in previous studies [20,54], where they reported an optical gap of about 0.2 eV [54] and a band gap of about 0.3 eV in their LDA + DMFT calculation [20]. Considering the fact that HF usually overestimates the

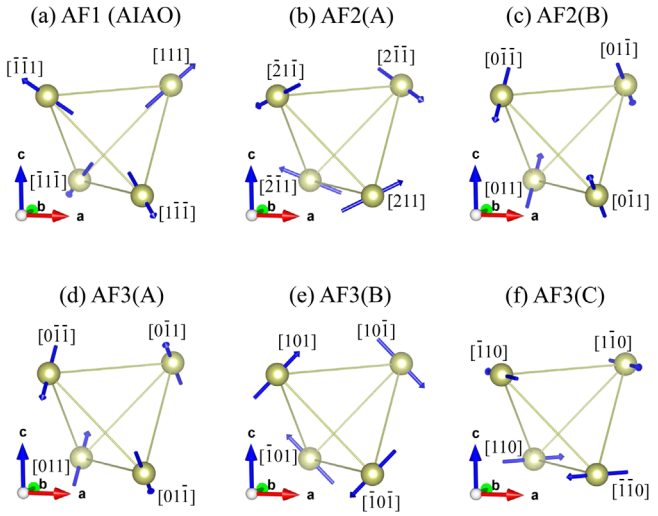

FIG. 1. (a) AF1, the AIAO antiferromagnetic configuration, all the magnetic moments point to (against) the center of the tetrahedron. (b),(c) AF2, other twofold degenerate antiferromagnetic configurations. (d),(e),(f) AF3, other threefold degenerate antiferromagnetic configurations.

band gap, here we choose a value $U = 1.1$ eV which will induce a little larger band gap of about 0.4 eV [41]. A phase diagram with Hund's coupling J_H at $J_H/U = 0.2$ is also calculated and plotted in the Supplemental Material [41]. It turns out that Hund's coupling does not change the overall phase diagram because there is only one hole per Ir site in t_{2g} subspace.

To study the possible nonlinear magnetization discussed in Ref. [55] and reported in Ref. [35], we apply an external magnetic field $\vec{H}$ in the [001] plane and continuously rotate it by 2π, and then calculate the net magnetic moments along [001] direction M^{001} induced by the transverse magnetic field. M^{001} as a function of the rotation angle θ are plotted in Fig. 3 for the AF1 and AF3 phases at $U = 1.1$ and $\lambda = 0.4$ eV. We only plot M^{001} for one of the two time-reversal partners, and M^{001} for the other partner will have the same magnitude but with opposite sign. Our numerical results are consistent with the experimental results, where the nonlinear magnetization pattern was rotated by 45° under the field cooling process [35]. The calculated M^{001} shows a d_{xy} pattern for AF1, which is corresponding to the results in Figs. 2(a), 2(b) in Ref. [35] where the field $\boldsymbol{H}_{\rm fc}$ is along the $[\bar{1}\,\bar{1}\,0]$ direction. While M^{001} shows a $d_{x^2-y^2}$ pattern for AF3(C), which is corresponding to the results in Figs. 2(c), 2(d) in Ref. [35], where the field $\boldsymbol{H}_{\rm fc}$ is along the $[\bar{1}10]$ direction. Note that the measured nonlinear magnetization in Ref. [35] show distorted d waves, which may be caused by an additional order that already exists at 300 K. M^{001} for the AF3(A) and AF3(B) configurations are zero due to the symmetry reason. The occurrence of the additional metastable magnetic phase AF3 can explain the observed $\pi/4$ phase shift of the magnetization pattern with the assumption that the field cooling processes may stabilize AF3.

Figure 2(b) is the phase diagram for the ideal pyrochlore structure without any distortion. We find that the two-dimensional $c\Gamma_{5+}$ representation [AF2 in Figs. 1(b), 1(c)] is always the ground state, which is quite different with the situation in the distorted structure. AF3 and AF1 are both locally stable metastable states here and can also coexist with AF2 in some parameter region. The total energy of all the three phases satisfies $E_{\rm tot}(\mathrm{AF2}) < E_{\rm tot}(\mathrm{AF3}) < E_{\rm tot}(\mathrm{AF1})$. The color map is used to label the total energy difference between AF3 and AF2: $E_{\rm tot}(\mathrm{AF3}) - E_{\rm tot}(\mathrm{AF2})$ (with units

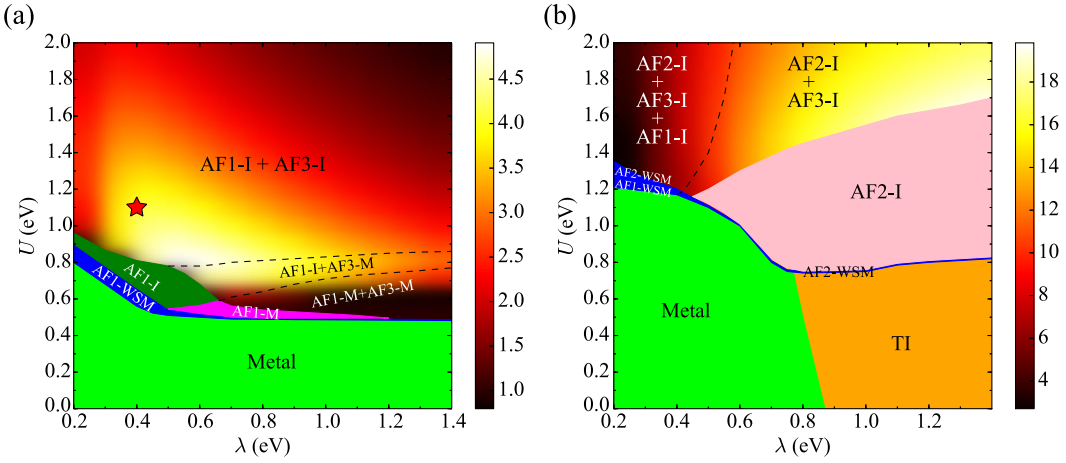

FIG. 2. The phase diagram as a function of Coulomb interaction U and SOC λ. (a) For the distorted structure, the ground magnetic state is always AF1. AF3 can coexist with AF1 in a very large region. The color map is used to label their total energy difference: $E_{\rm tot}(\mathrm{AF3}) - E_{\rm tot}(\mathrm{AF1})$ (with units of meV). The red star indicates the reasonable parameters $U = 1.1$ eV and $\lambda = 0.4$ eV for real material of $Eu_2Ir_2O_7$. (b) For the nondistorted structure, the ground magnetic state is always AF2. AF3 and AF1 can coexist with AF2 in some regions. The color map is used to label the total energy difference between AF3 and AF2: $E_{\rm tot}(\mathrm{AF3}) - E_{\rm tot}(\mathrm{AF2})$ (with units of meV). Antiferromagnetic (AF), insulator (I), metal (M), Weyl semimetal (WSM), and topological insulator (TI).

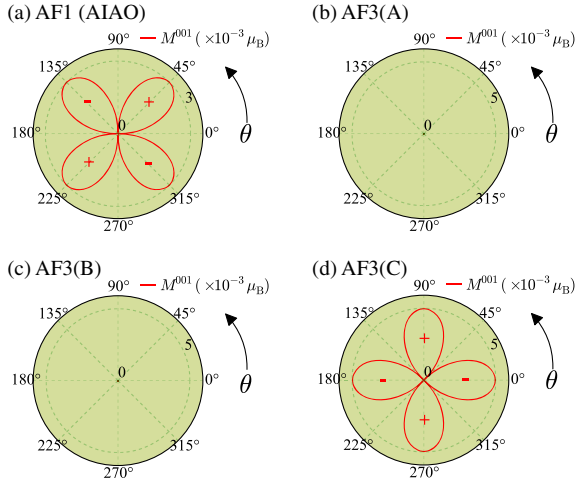

FIG. 3. The net magnetic moments along the [001] direction M^{001} as a function of the rotation angle θ at $U = 1.1$ and $\lambda = 0.4$ eV for (a) AF1 and (b),(c),(d) AF3.

of meV). These results indicate that a large enough trigonal distortion [56] may be crucial for stabilizing the AIAO state. For most of the pyrochlore iridates, the trigonal distortion is indeed large enough, which implies that the AIAO is likely to be the ground state.

In the antiferromagnetic phase of the distorted structure, we expand the local density matrix ρ to measure the weights of the OPs. We plot their weights as a function of λ for the AF1 and AF3(C) phases at $U = 1.1$ eV in Fig. 4. The new finding of our calculations is that, besides large dipoles, there also exist considerable higher-rank octupolar moments.

In the AF1 phase, the dipoles are $O_{10}^{13} = l_z/2$ and $O_{01}^{13} = \sqrt{2/3}s_z$. Besides these dipoles, there is another spin-orbital coupled dipole O_{21}^{1} [57,58] with O_{21}^{11}, O_{21}^{12}, and O_{21}^{13} being the x, y, and z components (Eqs. S45–S47 in the Supplemental Material [41]). In the AF1 phase, the nonzero component is O_{21}^{13}. In the AF3(C) phase, the nonzero components of dipoles are $O_{10}^{12} = l_y/2$, $O_{01}^{12} = \sqrt{2/3}s_y$ and O_{21}^{12}. The arrows on the right side of Figs. 4(a), 4(b) mark the expectation values of the components of O_{10}^{1} (blue), O_{01}^{1} (green), and O_{21}^{1} (red) in the ideal atomic $j_{\text{eff}} = 1/2$ state (large SOC limit). At small SOC, their expectation values deviate quite far away from their atomic limits, and approach the atomic limits with the increment of SOC. At $U = 1.1$ and $\lambda = 0.4$ eV, the calculated ratio $\langle L_z\rangle/\langle S_z\rangle$ is about 2.3 for AF1 and the ratio $\langle L_y\rangle/\langle S_y\rangle$ is about 6.8 for AF3(c), which deviates quite far away from the value 4 in the atomic $j_{\text{eff}} = 1/2$ states [59,60]. These results indicate that the mixing of $j_{\text{eff}} = 1/2$ and $j_{\text{eff}} = 3/2$ states is indeed significant in $Eu_2Ir_2O_7$ and the $j_{\text{eff}} = 1/2$ single orbital picture is not applicable here.

The octupoles are defined as the components of a rank-3 irreducible tensor. We find two components O_{21}^{33} and O_{21}^{37} (Eq. S55 and Eq. S59 in the Supplemental Material [41]) with nonzero weights in the AF1 phase, and three components O_{21}^{34}, O_{21}^{35}, and O_{21}^{36} (Eqs. S56-S58 in the Supplemental Material [41]) in the AF3(C) phase. As shown in Fig. 4, for both AF1 and AF3(C) phases, with the realistic SOC strength ($\lambda = 0.4$ eV) the octupole weight can be comparable with the dipoles and cannot be ignored. With the increment of SOC, the octupole weights will vanish gradually and the magnetic moments of iridium ions can be described by the dipole moments only formed within the $j_{\text{eff}} = 1/2$ subspace in the strong SOC limit. We would emphasize that the mixing of $j_{\text{eff}} = 1/2$ and $j_{\text{eff}} = 3/2$ subspaces to some extent is the prerequisite for the occurrence of octupoles because $j_{\text{eff}} = 1/2$ subspace alone can only induce multipolar moments up to rank-1. We also note that the size ratio of octupoles and dipoles in the AF3 phase is a little larger than that in the AF1 phase, implying that the effective spin-orbit coupling $\langle \mathbf{L}\cdot\mathbf{S}\rangle$ would be smaller in AF3 than in AF1. This change may be seen in the XAS Ir L_2/L_3 branching ratio [59,61]. The occurrence of

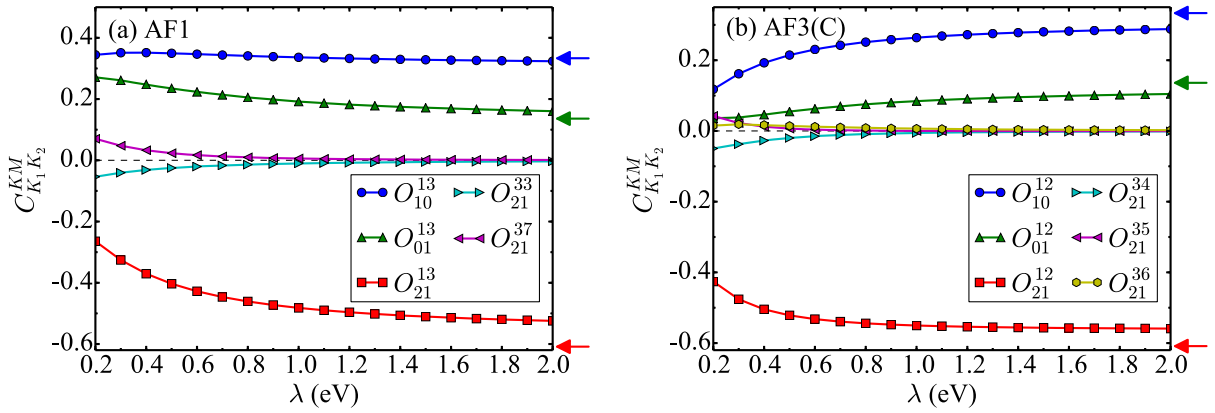

FIG. 4. The weights of OPs as a function of λ in the experimental structure with distortion at $U = 1.1$ eV for (a) AF1 and (b) AF3(C). The arrows indicate the expectation values of orbital (blue), spin (green), and orbital-spin (red) coupled dipoles in the atomic $j_{\text{eff}} = 1/2$ state, respectively.

these octupolar moments may bring some interesting physical consequence, which needs further study.

In summary, we have found a stable AIAO magnetic ground state in $Eu_2Ir_2O_7$ only when the trigonal lattice distortion is fully considered. Besides AIAO, a metastable magnetic phase AF3 with very close energy to AIAO is also found. The appearance of the AF3 phase can explain the nonlinear magnetization behavior in $Eu_2Ir_2O_7$ under field cooling. In the magnetic phase, besides large dipoles, we also find high-order multipolar octupoles with considerable amplitude. These results of $Eu_2Ir_2O_7$ serve as an example and can be used to explain the magnetic properties for other pyrochlore iridates.

Y. L. W. acknowledges the helpful discussions with Dr. Jianzhou Zhao and Rui Yu about the calculations. X. D. acknowledges the helpful discussions with Professor Nai Phuan Ong, Dr. Tian Liang, and Professor Hiroshi Shinaoka. L. F. thanks Timothy Hsieh for valuable discussions. This work is supported by the National Basic Research Program of China (Grant No. 2013CB921700). L. F. is supported by DOE Office of Basic Energy Sciences, Division of Materials Sciences and Engineering under Award No. DE-SC0010526.

[1] M. Imada, A. Fujimori, and Y. Tokura, Rev. Mod. Phys. **70**, 1039 (1998).
[2] P. Santini, S. Carretta, G. Amoretti, R. Caciuffo, N. Magnani, and G. H. Lander, Rev. Mod. Phys. **81**, 807 (2009).
[3] W. Witczak-Krempa, G. Chen, Y. B. Kim, and L. Balents, Annu. Rev. Condens. Matter Phys. **5**, 57 (2014).
[4] N. Taira, M. Wakeshima, and Y. Hinatsu, J. Phys. Condens. Matter **13**, 5527 (2001).
[5] J. S. Gardner, M. J. P. Gingras, and J. E. Greedan, Rev. Mod. Phys. **82**, 53 (2010).
[6] X. Wan, A. M. Turner, A. Vishwanath, and S. Y. Savrasov, Phys. Rev. B **83**, 205101 (2011).
[7] W. Witczak-Krempa and Y. B. Kim, Phys. Rev. B **85**, 045124 (2012).
[8] S. M. Disseler, C. Dhital, A. Amato, S. R. Giblin, C. de la Cruz, S. D. Wilson, and M. J. Graf, Phys. Rev. B **86**, 014428 (2012).
[9] W. Witczak-Krempa, A. Go, and Y. B. Kim, Phys. Rev. B **87**, 155101 (2013).
[10] S. Zhao, J. M. Mackie, D. E. MacLaughlin, O. O. Bernal, J. J. Ishikawa, Y. Ohta, and S. Nakatsuji, Phys. Rev. B **83**, 180402 (2011).
[11] H. Shinaoka, S. Hoshino, M. Troyer, and P. Werner, Phys. Rev. Lett. **115**, 156401 (2015).
[12] G. Prando, R. Dally, W. Schottenhamel, Z. Guguchia, S.-H. Baek, R. Aeschlimann, A. U. B. Wolter, S. D. Wilson, B. Büchner, and M. J. Graf, Phys. Rev. B **93**, 104422 (2016).
[13] D. Yanagishima and Y. Maeno, J. Phys. Soc. Jpn. **70**, 2880 (2001).
[14] K. Matsuhira, M. Wakeshima, R. Nakanishi, T. Yamada, A. Nakamura, W. Kawano, S. Takagi, and Y. Hinatsu, J. Phys. Soc. Jpn. **76**, 043706 (2007).
[15] B.-J. Yang and Y. B. Kim, Phys. Rev. B **82**, 085111 (2010).
[16] K. Matsuhira, M. Wakeshima, Y. Hinatsu, and S. Takagi, J. Phys. Soc. Jpn. **80**, 094701 (2011).
[17] J. J. Ishikawa, E. C. T. O'Farrell, and S. Nakatsuji, Phys. Rev. B **85**, 245109 (2012).
[18] F. F. Tafti, J. J. Ishikawa, A. McCollam, S. Nakatsuji, and S. R. Julian, Phys. Rev. B **85**, 205104 (2012).
[19] M. Sakata, T. Kagayama, K. Shimizu, K. Matsuhira, S. Takagi, M. Wakeshima, and Y. Hinatsu, Phys. Rev. B **83**, 041102 (2011).
[20] H. Zhang, K. Haule, and D. Vanderbilt, Phys. Rev. Lett. **118**, 026404 (2017).
[21] Y. Machida, S. Nakatsuji, Y. Maeno, T. Tayama, T. Sakakibara, and S. Onoda, Phys. Rev. Lett. **98**, 057203 (2007).
[22] Y. Machida, S. Nakatsuji, S. Onoda, T. Tayama, and T. Sakakibara, Nature (London) **463**, 210 (2010).
[23] X. Hu, A. Rüegg, and G. A. Fiete, Phys. Rev. B **86**, 235141 (2012).
[24] D. Pesin and L. Balents, Nat. Phys. **6**, 376 (2010).
[25] A. B. Sushkov, J. B. Hofmann, G. S. Jenkins, J. Ishikawa, S. Nakatsuji, S. Das Sarma, and H. D. Drew, Phys. Rev. B **92**, 241108 (2015).
[26] G. Chen and M. Hermele, Phys. Rev. B **86**, 235129 (2012).
[27] M. Kargarian, J. Wen, and G. A. Fiete, Phys. Rev. B **83**, 165112 (2011).
[28] M. Kurita, Y. Yamaji, and M. Imada, J. Phys. Soc. Jpn. **80**, 044708 (2011).
[29] H.-M. Guo and M. Franz, Phys. Rev. Lett. **103**, 206805 (2009).
[30] Q. Chen, H.-H. Hung, X. Hu, and G. A. Fiete, Phys. Rev. B **92**, 085145 (2015).
[31] X. Hu, Z. Zhong, and G. A. Fiete, Sci. Rep. **5**, 11072 (2015).
[32] Y. Yamaji and M. Imada, Phys. Rev. X **4**, 021035 (2014).
[33] E. Y. Ma, Y.-T. Cui, K. Ueda, S. Tang, K. Chen, N. Tamura, P. M. Wu, J. Fujioka, Y. Tokura, and Z.-X. Shen, Science **350**, 538 (2015).
[34] Y. Yamaji and M. Imada, Phys. Rev. B **93**, 195146 (2016).
[35] T. Liang, T. H. Hsieh, J. J. Ishikawa, S. Nakatsuji, L. Fu, and N. P. Ong, Nat. Phys. **13**, 599 (2017).
[36] L. Zhao, D. H. Torchinsky, H. Chu, V. Ivanov, R. Lifshitz, R. Flint, T. Qi, G. Cao, and D. Hsieh, Nat. Phys. **12**, 32 (2016).
[37] J. N. Millican, R. T. Macaluso, S. Nakatsuji, Y. Machida, Y. Maeno, and J. Y. Chan, Mater. Res. Bull. **42**, 928 (2007).
[38] G. Kresse and J. Furthmüller, Phys. Rev. B **54**, 11169 (1996).
[39] N. Marzari, A. A. Mostofi, J. R. Yates, I. Souza, and D. Vanderbilt, Rev. Mod. Phys. **84**, 1419 (2012).
[40] A. A. Mostofi, J. R. Yates, Y.-S. Lee, I. Souza, D. Vanderbilt, and N. Marzari, Comput. Phys. Commun. **178**, 685 (2008).
[41] See Supplemental Material at http://link.aps.org/supplemental/10.1103/PhysRevLett.119.187203 for the computational details, the definition of the local *XYZ* coordinate and local [111] *xyz* coordinate, the definition of multipolar order parameters, the phase diagram with Hund's coupling and band structures, which includes Refs. [42–48].

[42] P. E. Blöchl, Phys. Rev. B **50**, 17953 (1994).
[43] G. Kresse and D. Joubert, Phys. Rev. B **59**, 1758 (1999).
[44] J. P. Perdew, K. Burke, and M. Ernzerhof, Phys. Rev. Lett. **77**, 3865 (1996).
[45] X. Y. Deng, L. Wang, X. Dai, and Z. Fang, Phys. Rev. B **79**, 075114 (2009).
[46] The OpenMX code is available at http://www.openmx-square.org/.
[47] T. Kondo, M. Nakayama, R. Chen, J. J. Ishikawa, E.-G. Moon, T. Yamamoto, Y. Ota, W. Malaeb, H. Kanai, Y. Nakashima, Y. Ishida, R. Yoshida, H. Yamamoto, M. Matsunami, S. Kimura, N. Inami, K. Ono, H. Kumigashira, S. Nakatsuji, L. Balents, and S. Shin, Nat. Commun. **6**, 10042 (2015).
[48] M. Nakayama, T. Kondo, Z. Tian, J. J. Ishikawa, M. Halim, C. Bareille, W. Malaeb, K. Kuroda, T. Tomita, S. Ideta, K. Tanaka, M. Matsunami, S. Kimura, N. Inami, K. Ono, H. Kumigashira, L. Balents, S. Nakatsuji, and S. Shin, Phys. Rev. Lett. **117**, 056403 (2016).
[49] K. Blum, *Density Matrix Theory and Applications*, 3rd ed., Springer Series on Atomic Optical and Plasma Physics (Springer, Berlin, 2012).
[50] A. S. Wills, M. E. Zhitomirsky, B. Canals, J. Sanchez, P. Bonville, P. D. de Rotier, and A. Yaouanc, J. Phys. Condens. Matter **18**, L37 (2006).
[51] H. Sagayama, D. Uematsu, T. Arima, K. Sugimoto, J. J. Ishikawa, E. O'Farrell, and S. Nakatsuji, Phys. Rev. B **87**, 100403 (2013).
[52] H. Takatsu, K. Watanabe, K. Goto, and H. Kadowaki, Phys. Rev. B **90**, 235110 (2014).
[53] S. M. Disseler, Phys. Rev. B **89**, 140413 (2014).
[54] K. Ueda, J. Fujioka, and Y. Tokura, Phys. Rev. B **93**, 245120 (2016).
[55] T.-h. Arima, J. Phys. Soc. Jpn. **82**, 013705 (2013).
[56] D. Uematsu, H. Sagayama, T.-h. Arima, J. J. Ishikawa, S. Nakatsuji, H. Takagi, M. Yoshida, J. Mizuki, and K. Ishii, Phys. Rev. B **92**, 094405 (2015).
[57] P. Carra, B. T. Thole, M. Altarelli, and X. Wang, Phys. Rev. Lett. **70**, 694 (1993).
[58] J. Luo, G. T. Trammell, and J. P. Hannon, Phys. Rev. Lett. **71**, 287 (1993).
[59] M. A. Laguna-Marco, D. Haskel, N. Souza-Neto, J. C. Lang, V. V. Krishnamurthy, S. Chikara, G. Cao, and M. van Veenendaal, Phys. Rev. Lett. **105**, 216407 (2010).
[60] S. Fujiyama, H. Ohsumi, K. Ohashi, D. Hirai, B. J. Kim, T. Arima, M. Takata, and H. Takagi, Phys. Rev. Lett. **112**, 016405 (2014).
[61] J. P. Clancy, N. Chen, C. Y. Kim, W. F. Chen, K. W. Plumb, B. C. Jeon, T. W. Noh, and Y.-J. Kim, Phys. Rev. B **86**, 195131 (2012).